Effect of Various Duct Shapes and Blade Sections on the Efficiency Performance of Horizontal Axis Tidal Current Turbine

Mahdi Azimi Gandomani [1]
Hassan Ghassemi [1,2]
Guanghua He [3]

[1] Marine and Hydrokinetic Energy Group, Department of Maritime Engineering, Amirkabir University of Technology (AUT), Tehran, Iran

[2] Int. School of Ocean Science and Engineering, Harbin Institute of Technology (HIT), Weihai, China, Ira

[3] Int. School of Ocean Science and Engineering, Harbin Institute of Technology (HIT), Weihai, China

* Corresponding author: *gasemi@aut.ac.ir (Hassan Ghassemi)*

ABSTRACT

This research emphasizes the importance of optimal design for tidal turbines under various ducts and blade sections to enhance efficiency. A Reynolds-Averaged Navier-Stokes (RANS) solver with turbulence model is used to investigate the performance of horizontal-axis tidal current turbines (HATCT) under different ducts and blade sections. Analyses were conducted using various meshes and, in several stages, to ensure the accuracy of the results. Six types of different blades sections and winglets are selected and the numerical results of thrust, torque and power coefficients are compared. demonstrating the accepTable accuracy of this analytical method. It is indicated that the effect of the winglet caused to increase the power coefficient. The numerical results were compared and validated with experimental data and found in good agreement. Finally, the effect of the different duct shapes with turbine type 1 at TSR = 5 is obtained with significant results of the power coefficient.

Keywords: Horizontal axis tidal current turbine (HATCT), Duct shapes, Blade sections, Hydrodynamic performance, Power coefficient.

INTRODUCTION

Tidal energy, as one of the renewable energy sources, has a high potential to help solve problems related to the increasing need for energy, environmental pollution, climate change, limitations of fossil fuels, and their rising costs. This type of energy, which is derived from the regular changes in the sea and ocean water levels due to the gravitational pull of the moon and sun, has a high predictability and reliable access. Extensive research is being conducted to improve technologies related to tidal turbines and reduce their costs, to make wider use of this clean and sustainable energy source possible. Tidal energy can be considered a clean energy source, as it does not have a negative impact on the environment and ecosystems [1]. This energy is among the available and reliable energies. Tidal energy is

generated by the tides. Due to the vastness of seas and oceans, it is produced in a significant amount. By placing turbines in the direction of water flow, the rise and fall of water caused by tides, tidal energy can be converted into electrical energy. The extraction of this energy is more common in suiTable estuaries and waterways [2]. For this reason, tidal turbine farms are used to generate energy. A tidal turbine farm, comparable to a wind farm, consists of multiple tidal turbines set up in regions with significant tidal activity to capture the kinetic energy from tidal currents. These installations are submerged in areas known for consistent and strong water movements, such as estuaries, coastal regions, or narrow channels between landmasses. Fig. 1 (a) and (b) depict a tidal turbine farm and AR1500. SIMEC Atlantis Energy has redeployed its 1.5MW tidal energy turbine (AR1500) at its MeyGen site offshore Scotland. The MeyGen site

is the largest fully consented tidal stream site in the world and SIMEC Atlantis is continuing to work with the UK Government and industry partners to unlock its full potential, delivering a 400MW green and predicTable power station [3]. Tidal turbines can convert tidal energy into mechanical energy, and through a generator, this energy is converted into electricity [4]. These turbines increase the flow rate using a duct, which results in the production of more power [5]. The design and construction of tidal turbines is an active industrial field in various countries. Using these turbines, it is possible to create a power plant that serves as a renewable marine energy source [6,7].
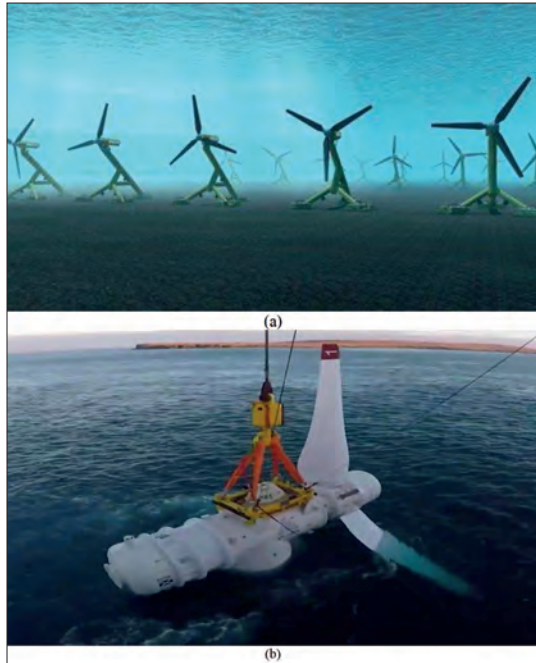

Fig. 1. (a) A farm of tidal turbine, b) Tidal turbine AR-1500 [3].

For horizontal axis tidal current turbine (HATCT), blade element momentum theory (BEMT) and Computational Fluid Dynamics (CFD) simulation are used to calculate hydrodynamic parameters. CFD modeling, which is connected to the rotational movement of a rotor with one degree of freedom, is a suiTable solution for predicting the time-dependent performance of kinetic energy turbines [8,9]. In 2012, Bahaj et al. studied the flow sequence design of an axial kinetic energy turbine. They tested an axial rotor that had two rows of blades [10]. The research by song et al showed the development and assessment of three tidal stream turbine designs, each with a capacity of 100 kW. The process begins with the creation of a foundational blade model, guided by conventional wind turbine design principles. [11]. The study by Muratoglu aims to conducted a numerical performance analysis on pre-designed blade sections for hydrokinetic turbines. he examined the lift, drag, and pressure coefficients of different NACA, NREL, and RISØ hydrofoils [12]. Schleicher and his colleagues designed a two-bladed rotor for a kinetic energy water turbine. They used ANSYS-Fluent software for fluid flow simulation [13]. They showed that using guide blades between turbine stages increases the turbine efficiency by nine percent. Shojaei Fard et al. numerically simulated a small axial water turbine in CFX software. They used fine and coarse computational grids and compared the numerical results with experimental data [14]. The research by Rahimian showed that CFD models can effectively simulate turbine performance with appropriate numerical methods. It also assessed how different numerical approached affect the prediction of a two-bladed turbine model's performance using towing tank data from the USNA [15]. a study explored suiTable methodologies and approaches to simulate the hydrodynamic performance of horizontal marine turbines, focusing on flow separation phenomena [16]. Alipour et al carried out the hydrodynamic performance of the HATCT under different blade pitch angles [17] and blade number [18]. Their results indicated that at higher values of blade pitch angle; by increasing the thickness, the maximum amount of torque enhances. Furthermore, the augmentation in the TSR led to an increase in maximum C_p at the lower value of blade pitch angle under different current velocity [19]. Also, an experimental investigation presented into the performance of a three-bladed HATCT model operating under different wave-current combinations [20].

For ducted HATCT, a combination of BEMT and CFD may determine the induction velocity in the duct. However, integrating BEMT with CFD complicates the process, leading to a significant increase in design time. Previous studies on ducted turbines mainly focused on one-sided flow [21] or used an actuator disk to simulate the turbine section, without proposing a design method for bidirectional turbines [22, 23]. The ducted type is anticipated to enhance performance during turbine start-up and tidal velocity variations [24]. Lawn analyzed the performance of ducted axial turbines using one-dimensional flow theory analytically [25]. Setoguchi tried in the field of designing and constructing a double-wall diffuser and found that the shape of the diffuser is an important factor in increasing turbine efficiency [26]. Other researchers like Jo et al. [27] and Shives et al. [28] worked respectively on the flow velocity drop through the ducted turbine and efficiency calculation in CFX software. In 2020, Im et al. presented designs for blades and a water velocity amplification device for the development of a 5-kW duct-type floating tidal current turbine [29]. Tsuru worked on research that using ducted turbine power as the design condition, the tangential velocity difference between the front and rear of the turbine was calculated using Euler's equation. The blade stagger angle was determined based on potential flow theory [30].

In our Marine and Hydrokinetic Energy (MHE) group at AUT, we conducted comprehensive research on the different configurations of the tidal turbines, such as new profiles at the leading-edge tubercles [31], impact of the duct and number of blades [32], featuring various blade shapes and twist angles [33, 34], a counter-rotating tidal turbine with and without duct [35].

In this paper, we have been focused on exploring the available methods to increase the torque and power by utilizing on the blade sections and duct profiles. The effects of different configurations on the duct and blades by adding a winglet at the tip, changing at the trailing edge of the blade and duct, as well as laced duct have been investigated to enhance power coefficient.

METHODOLOGY

The Navier-Stokes equations, fundamental in fluid dynamics, describe the motion of fluid substances. Through Reynolds averaging, these equations can be decomposed into mean and fluctuating components, a process that forms the basis of the Reynolds-averaged Navier-Stokes (RANS) method. This approach allows for the analysis of turbulent flows by averaging the effects of the turbulence over time, making the complex Navier-Stokes equations more manageable for practical engineering applications, such as studying the hydrodynamics of tidal turbines.

In the context of RANS, the hydrodynamics of a tidal turbine can be addressed using the incompressible Navier-Stokes equations. The RANS equations are further simplified and made solvable through the application of turbulence models, with the $k-\omega$ (kinetic energy - specific dissipation rate) model being a noTable example. This two-equation model is particularly adept at handling streamwise pressure gradients and accurately modeling the viscous near-wall region, which are critical aspects in the study of tidal turbine performance. The $k-\omega$ model enhances the robustness and accuracy of the flow simulation, especially in accounting for wall effects, which are pivotal in determining the flow dynamics around the turbine blades.

The $k-\omega$ SST (shear stress transport) turbulence model, utilized in the study referenced (Ghafari et al. 2022), further refines the approach by effectively capturing the free-stream vorticity's impact outside the shear layer, thereby improving the model's predictive capability regarding the turbulent flow characteristics. After using these methods, torque and power coefficientswere used to calculate hydrodynamic parameters.

Hydrodynamic of HATCT

A turbine is a device that rotates when immersed in a fluid stream of speed V. The desired effect is the establishment of a torque Q that keeps the blades in rotation and brings about the generation of a mechanical power by torque times angular velocity ($P = Q.\omega$). An important state variable of the turbine is the Tip Speed Ratio (TSR), i.e., the ratio of the tip speed to current speed ($TSR = \frac{\omega R}{V}$), where R being the turbine radius and V is the current speed. The power coefficient (C_p) is defined as:

$$C_P = \frac{P}{0.5\rho V^2 A} \tag{1}$$

where P is the generated power, A is the area of a reference surface ($A = \pi R^2$), and ρ is the water density. Similarly, the torque coefficient (C_Q) is defined as:

$$C_Q = \frac{Q}{0.5\rho RV^2 A} = \frac{C_P}{TRS} \tag{2}$$

where Q is the torque at the turbine hub. Finally, the thrust coefficient (C_T) has the following expression:

$$C_T = \frac{T}{0.5\rho RV^2 A} \tag{3}$$

where T is the turbine thrust, that is the axial force developed by the device immersed in the flow and functioning at a given TSR.

The area A in the above definitions is always taken coincident with the bare rotor disk surface area, both for the bare turbine and for the diffuser-augmented one. This is important when comparing performance of different solutions in terms of efficiency.

Geometry of HATCT

The main basis of the turbine sections designed in this paper is adapted from the published paper by Song et al. [11], which initially involves designing and validating the turbine presented in the article, and then using it to design new types with different profiles and changing the twist angle to achieve the highest efficiency and the most optimal results. The turbine mentioned in the article (Song et al) is Type 1 that shown in Table 1, which is designed for validation both with and without a guide vane. The angles used in Types 2 and 3 are obtained through multiple simulations conducted at different angles rather than Type 1, in such a way to achieve the highest efficiency.

In this research, in addition to three types (1, 2 and 3), other changes have been made to the appearance of the blades to increase their efficiency. For this purpose, one type has been added a winglet to the end of its radius (Types 4 and 5), and another type has been given a sinusoidal shape at the trailing edge (Type 6). The winglet is applied at the blade tip with 2%R rake and rounding shape. All these six types have been simulated after validation to determine the impact of the changes made. The general specifications of the various proposed tidal turbine types are presented in Table 1.

Tab. 1. Various proposed types of tidal turbine (HATCT).

Type No.	Blade Section	Note
Type-1	NACA63-418	Original blade section (Based on Song et al. 2012)
Type-2	NACA653618	Change in blade section
Type-3	S830	Change in blade section
Type-4	NACA63-418	Blade with winglet
Type-5	S830	Blade with winglet
Type-6	S830	Trailing edge have sinusoidal shape

NUMERICAL IMPLEMENTATION AND VALIDATION

Computational domain

The computational domain for the simulation is divided into two regions: an outer region and an inner region, which are considered as the stationary and rotating domains, respectively. The computational domain and their moving and stationary regions are presented in the Fig. 2. For the outer

region, a cylindrical domain with a height of 5R upstream, 15R downstream, and a cylinder radius of 5R, scaled to the turbine radius, is employed. The rotating domain is a cylindrical shape with a radius of 1.1R and a height of 0.25R, where R is the radius of the rotor.
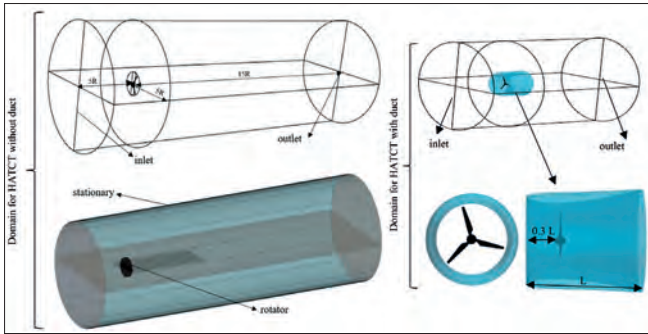

Fig. 2. Computational domain and boundary conditions.

Mesh Generation

Selecting an appropriate mesh for the computational domain is one of the key steps in the numerical simulation process. Using a suiTable mesh can significantly impact the accuracy and solution time of the problem. Generally, the more precise and appropriately patterned the mesh is designed, the faster and more accurate the analysis will be. The STAR-CCM+ software can generate high-quality structured and unstructured meshes for domains, using its automatic meshing tools and the latest available methods. For the rotating region, a polyhedral mesh has been used, and for the stationary region, a trimmed mesh has been utilized. Meshing around a duct and HATCT must be designed to accurately simulate water flow and turbulence effects. Examples of mesh designs for a HATCT's computational domain are illustrated in Fig. 3.
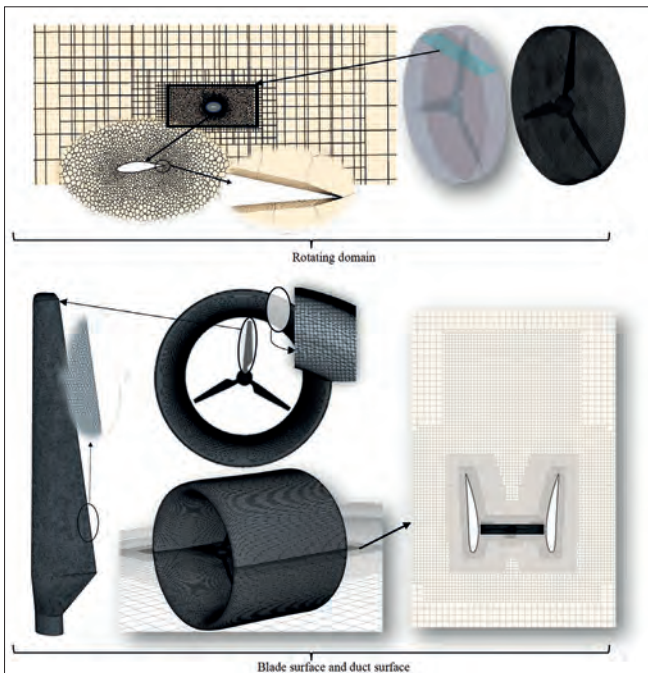
Fig. 3. Meshing of a section passing through the blade and blade surface and rotating domain and duct.

To create a regular grid in the external domain, this domain has been divided into several parts using a control volume. By using the available tools, the number of grid edges in the domain of the solved control has been managed. In Fig. 4, the grid of the external solution domain is displayed.
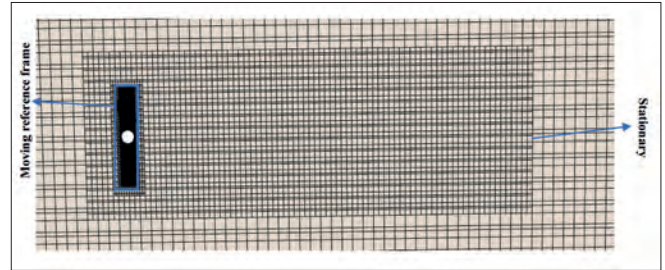

Fig. 4. Meshing the moving and stationary domain.

Boundary conditions

As shown in Table 2 and illustrated in Fig. 2, for the inlet and outlet locations, the boundary conditions of velocity inlet and pressure outlet have been considered. In the stationary domain, the boundary conditions are set as uniform inlet velocity and relative pressure at the outlet boundaries is set to zero. No-slip conditions are used for the hub and turbine blade surfaces. A common interface boundary between the stationary and rotating regions is utilized.

Tab. 2. Simulation boundary conditions.

Location	Setting	Mathematical formulation
Blades and hub	Wall, no-slip	$V_{wal} = 0$
Side	Symmetry	–
Inlet	Velocity inlet	$V_{intel} = flow\ speed$
Outlet	Pressure outlet	$P_{stat} = P_{specific}$

Validation

Validating numerical analyses is crucial for accuracy. Key aspects include:
- Ensuring mesh independence of results,
- Proper mesh sizing near objects, especially considering y+ values,
- Correct settings for boundary and domain conditions,
- Turbulence models, time steps, convergence criteria, and solver types.

For both stationary and rotating domains, multiple mesh size adjustments were made to determine the optimal number of meshes required. Comparing numerical results with experimental data ultimately confirms simulation accuracy.

Fig. 5 shows mesh independency of the C_Q and C_T of the turbine Type 1 at TSR = 5. As observed, the simulation process can be considered mesh independent beyond 4,900,000, because further increasing the number of meshes beyond that point does not change the result. Total number of meshes that we chose for simulations is equal to 4,900,000. For the simulations including Type 1 and duct, this number is approximately 6,500,000.
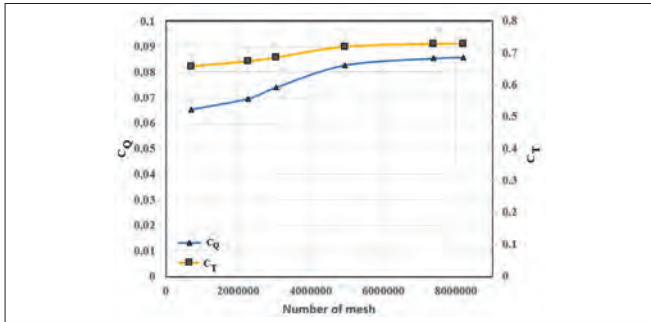
Fig. 5. Mesh independency for Type 1 (TSR=5).

The average value of y+ is about 5, which is accepTable for this simulation. The y+ Contour for the turbine Type 1 is presented in Fig. 6-a. Also, Fig. 6-b shows the y+ contour of one of the simulated ducts.
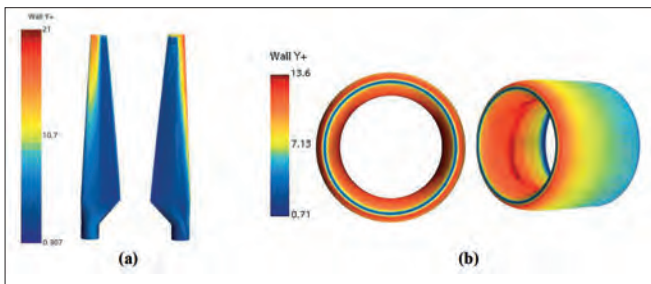

Fig. 6. (a) The y+ contours of HATCT Type 1.
(b) The y+ contours of duct no. 1 (TSR=5).

Here, the numerical results of the thrust, torque and power coefficients obtained from the numerical simulation are presented at different TSR (= $\frac{\omega R}{V}$) ranging from 3 to 10, assuming rotating speed of 270 RPM or 4.5 RPS ($\omega = \frac{2\pi n}{60}$ = 28.26 *rad/sec*) as a constant, and varying the current velocity *V* is from 0.9896 to 1.9792 m/s. Radius of rotor is 0.35 m, as given in Table 3.

For validation, the results obtained from the turbine simulation are compared with the article by Song et al [11]. In the conducted experiment, a horizontal-axis HATCT within the tip speed ratio (TSR) ranges of 5 to 10 was studied in the towing tank of the Pusan National University, South Korea. Validation for Type 1 and Type 4 have been compared between present numerical method and experimental data. As shown in Fig. 7, the obtained numerical results have a good correlation with experimental data. The numerical results are calculated at TSR ranges from 3 to 10. Maximum power coefficient of Type 1 and Type 4 are abstained 0.43 and 0.45 at around TSR = 5.4.
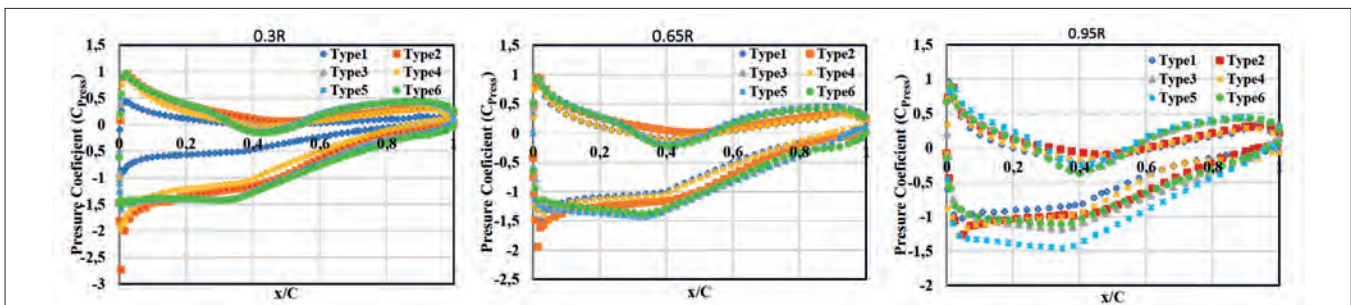
Tab. 3. Operation condition of the turbine. (n=4.5 RPS, R=0.35 m).

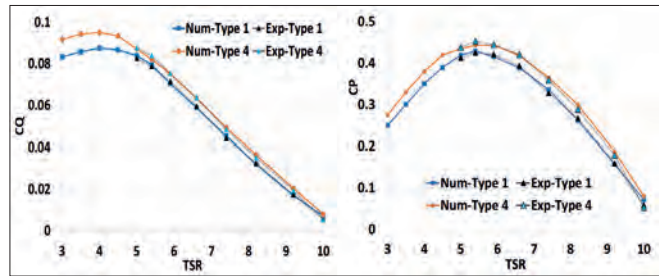| TSR	Velocity (m/s)
5	1.9792
5.4	1.8326
5.9	1.6773
6.6	1.4994
7.4	1.3373
8.3	1.2068
9.2	1.0757
10	0.9896

Fig. 7. Comparison between numerical results and experimental data for Types 1 and 4 (Experimental data is from Song et al. 2012 [11]).

RESULTS AND DISCUSSIONS

Pressure coefficient

The pressure coefficient (C_{Press}) is an essential parameter for calculation on the turbine blade surface. This coefficient is defined as follows:

$$C_{Press} = \frac{P_L - P_{ref}}{0.5\rho V_R^2} \qquad (4)$$

where P_{ref} is the reference hydrostatic pressure, P_L is the local pressure, and ρ is the fluid density. V_R is resultant velocity ($V_R = \sqrt{V^2 + (r\omega)^2}$).

The comparison of the pressure coefficient (at TSR = 5) for six turbine blade models at different radial sections (0.3R, 0.65R, 0.95R) from leading edge ($x/C = 0$) to trailing edge ($x/C = 1$) is presented in Fig. 8. As observed, the pressure coefficient for six different types is around $-2 < C_{Press} < +1$, the positive value is at face side and negative is back side. This different pressure causes to make a force and produce torque to rotate the rotor and generate power.

Pressure contours

Fig. 9 shows the pressure contours for Type 1 at TSR = 5 and TSR = 7.4, displaying the pressure in front and behind

Fig. 8. Pressure coefficient (C_{Press}) as a function of the chord ratio (x/C) at different radial (TSR = 5).

the blade (high pressure and low pressure) and the pressure at radial sections (0.3R, 0.65R, 0.95R). The pressure side of a HATCT blade is the side facing the flow of water, where the pressure is higher. The suction side is the side facing away from the flow, where the pressure is lower. The difference in the pressure distribution observed on the blades leads to different performance and efficiency for each type.
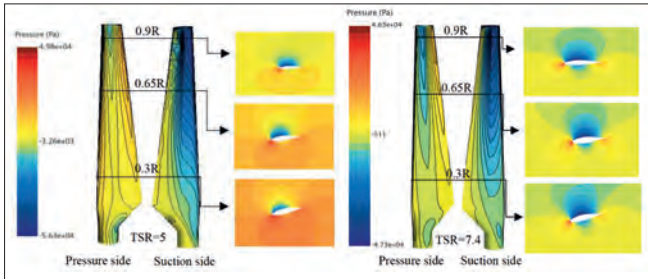

Fig. 9. Pressure contour of Type 1.

Hydrodynamic performance

The effects of changing the blade profile and adding winglets on the hydrodynamic performance of the HATCT are investigated. Fig. 10 shows the thrust, torque and power coefficients (C_T, C_Q and C_P) versus TSR for all 6 types of the different blade profiles. More power is obtained by type 5 and its maximum value is about 0.47 at TSR = 5.4 and all types have maximum at this TSR. With increasing the TSR from 5.4 to 10, the C_P decreases up to 0.06 at TSR = 10. Type 5 increases the and by approximately 11% at TSR = 5 compared to Type 1. Type 3 has increased the coefficients by approximately 4% compared to Type 1. Another effect by winglet, it is indicated that adding a winglet to Type 3 increases the C_P and C_Q by approximately 6% at TSR = 5. Additionally, Type 2 has increased the C_P and C_Q by approximately 2.5% compared to Type 1. Type 4 has almost the same efficiency as Type 6. it is observed that Type 5 (S830 with winglet) has higher efficiency than all other types, respectively Type 4, Type 6, Type 3, and Type 2 having higher efficiency than Type 1. Because of $C_P = C_Q . TSR$, trend of C_Q is almost the same as C_P. But for C_T is different. From TSR of 3 to 6 the C_T is increased and then it is slightly changed for all types. The maximum C_T is found for Type 5, its value is about 0.85 at TSR = 7.4, it is slightly decreased when TSR is increased.

Duct effect

Ducted turbines, also known as turbine diffusers, are engineering structures that enhance turbine efficiency. Placed at the turbine outlet, it may optimize the outflow pressure and velocity. Ducts are used in various turbine types, including wind, water, and gas turbines. Their design depends on turbine type, operating conditions, and efficiency goals. Ducts control outflow, reduce energy losses, and create pressure differences for increased energy production. For tidal turbines (HATCTs), selecting the right duct profile requires CFD analysis and field experiments to ensure compatibility with environmental conditions and energy production needs. After validating turbine simulations, research focus shifts to simulating the duct's impact on measured parameters. All ducts' sections are from NACA 4-digit profiles. We have simulated 11 types with different sections and shapes with the turbine type no 1. Fig. 11 is shown a typical duct and its dimensions. Chord length of the duct is 0.99 m and its inner and outer radiuses are 0.37 m and 0.51 m. The radius of the turbine is 0.35 and its gap between the tip of the rotor and duct is 0.02m. Fig. 12 shows 3-dimensional six different ducts.
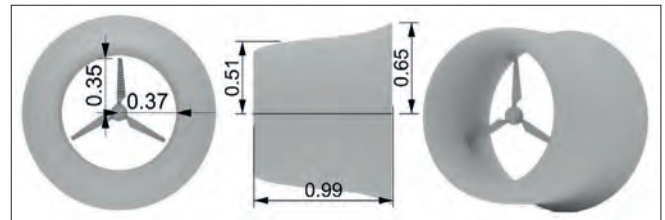

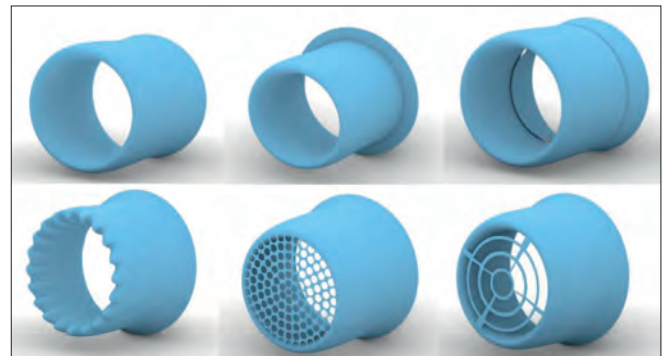*Fig. 11. Different view of the ducted turbine (gap is 0.02m).*

Fig. 12. Three-dimensional view of six different ducts.

Simulation carried out for all 11 ducted types with a turbine featuring the NACA63-418 (Type 1) profile at TSR = 5. These simulations were conducted after the validation of the turbine blade. the results presented in Table 4 and Fig. 13.
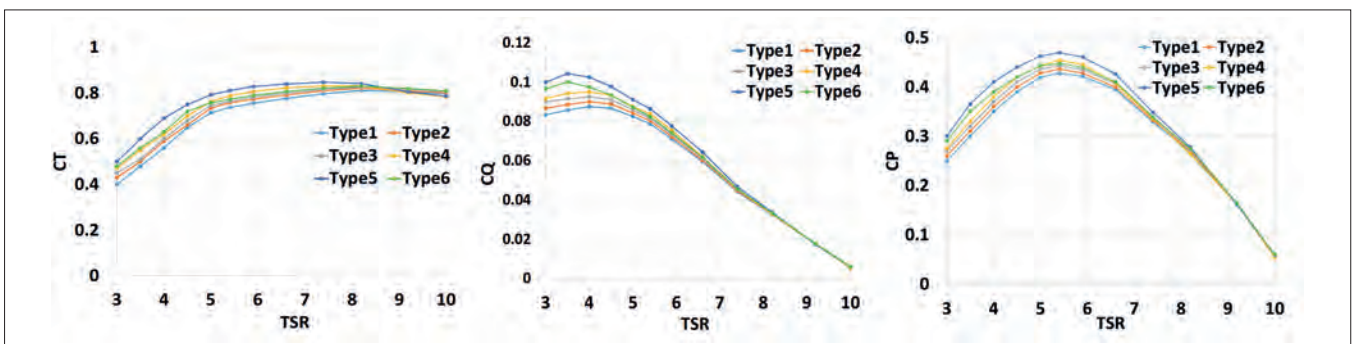

Fig. 10. Comparison of the thrust, torque and power coefficients (C_T, C_Q, C_P).

Tab. 4. Numerical results of Type 1 with 11 different ducts (TSR = 5).

| Type no.	Duct section	Profile shape	Duct angle (degree)	C_Q	C_P
1	NACA6615		5	0.1602	0.8056
2	NACA7715		5	0.165	0.8297
3	NACA7715-2		10	0.178	0.8951
4	NACA7715-with lace 1		10	0.035	0.1760
5	NACA7715-with lace 2		10	0.1019	0.5124
6	NACA7715-3		15	0.1827	0.9187
7	NACA7715-4		20	0.1758	0.8840
8	NACA8815		5	0.1668	0.8388
9	NACA6615 flapped		5	0.1428	0.7181
10	NACA6615 leading edge edit		5	0.1574	0.7915
11	NACA6615 trailing edge edit		5	0.1827	0.9187
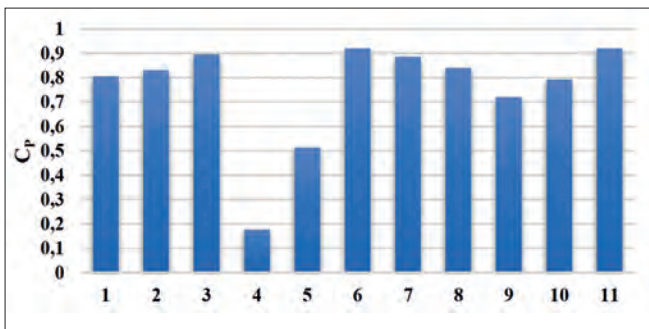
Fig. 13. power coefficient of turbine Type 1 with 11 different ducts, as shown in Table 5 (TSR=5)

Ducts no. 4 and 5 have lower efficiency compared to other types because they prevent the flow from passing through. It can even be observed that the first laced type has a negative effect. In the conclusion section, we will discuss and review the results of the ducts and the impact of parameters on turbine efficiency.

Streamlines, velocity and pressure of duct

In the following, the contours of streamlines, velocity and pressure for a few types are briefly presented. For a duct type (NACA7715-3), the pressure and velocity contours are shown in a horizontal section in Figs. 14 and 15, which allows for a clear observation of the pressure and velocity upstream and downstream.
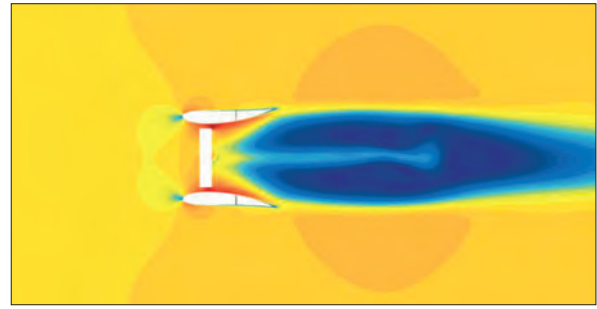

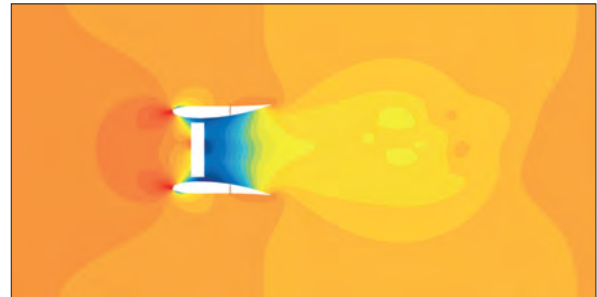Fig. 14. Velocity contour of a horizontal section passing through the duct.

Fig. 15. Pressure contour of a horizontal section passing through the duct.

In wind or tidal turbines, the diffuser expansion ratio (A_2/A_1) plays a critical role. It is determined by the ratio of the cross-sectional area at the diffuser's outlet (A_2) to that at its inlet (A_1). This ratio greatly influences the expansion of the flow within the diffuser, thereby affecting the turbine's efficiency. Fig. 16 presents the streamline with and without duct.
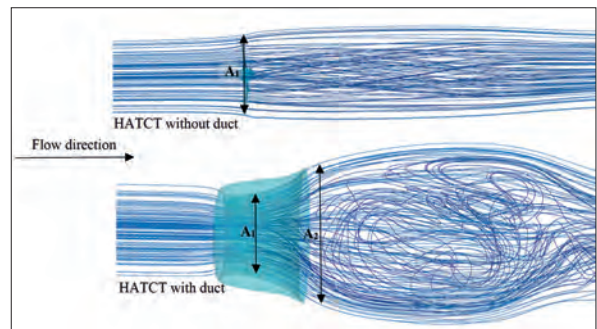

Fig. 16. Streamline of HATCT with and without duct.

Laced ducts are used in HATCTs design to protect turbines from debris and unwanted death of marine animals. Fig. 17 shows the axial velocity contour at 0.5R downstream of the turbine with a Lace duct, and shows the axial velocity contour at 0.5R upstream of the same turbine. As can be observed, due to having a lace, prevents the flow from passing through, which leads to a reduction in the extracted power.
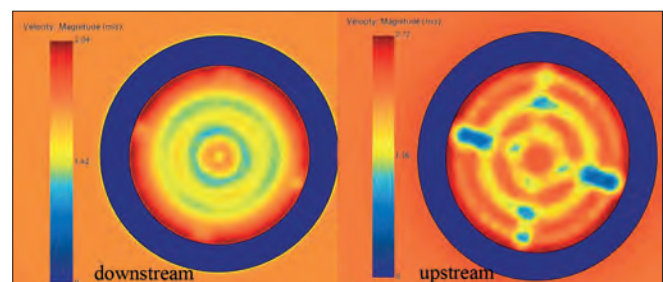

Fig. 17. Axial velocity contour at the distance of 0.5R upstream and at 0.5R downstream of the turbine.

Fig. 18 shows the pressure distribution contour on the laced duct. At the duct inlet, the pressure has increased due to the presence of a lace and then decreases upon hitting the turbine. At the outlet, the pressure has also increased. The velocity contour on a horizontal section is also presented in Fig. 19.
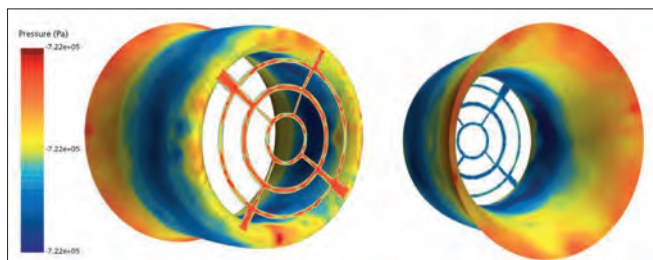

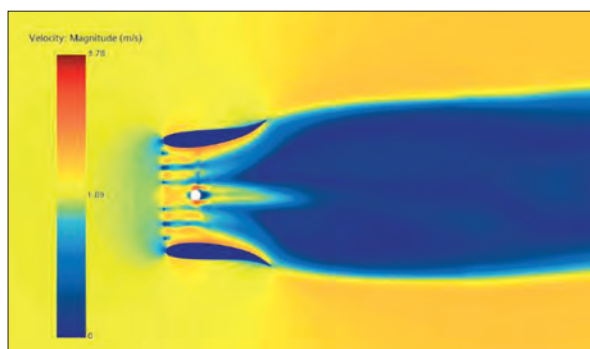*Fig. 18. Pressure contour on the surface of the laced duct.*

Fig. 19. Velocity contour from a horizontal section passing through the duct with lace.

CONCLUSIONS

The effect of the duct shape and blade sections were numerically investigated to find the hydrodynamic performance and power extraction of the HATCT. A finite volume-based RANS solver has been used to evaluate the performance of the different types. Validation was made through the comparison of both numerical results against experimental test data. Many results such as torque, thrust and power coefficients, pressure distribution on the blade and duct, flow behind the turbine were presented and discussed. The main results of this study are given as follows:

Blade section effect
- It was found that among the 6 different turbine types, type 5 is found the higher efficiency (0.47) at around TSR of 5.4. Also, all turbine types have maximum C_P at the same TSR.
- Pressure coefficient distribution at both face and back sides of the blade are given around +1 to -2 at three different radii (r/R = 0.3, 0.65 and 0.95) for all types. It is also shown that for all types the same trend are found in chordwise direction from leading edge to x/C = 0.4 and after that till trailing edge.

Duct shape effect
- Checking with different ducts at TSR = 5, it is found that the highest efficiency obtained for the duct 7715 with its angle of 15 [deg.].

- The influence of the camber, duct angle, zigzag shapes at LE and TE, and laced duct on the power coefficient were presented and discussed.
- Pressure, velocity and streamline are also demonstrated around the turbine and duct to ensure some phenomena.

NOMENCLATURES

A	Area
C_P	Power coefficient
C_Q	Torque coefficient
C_T	Thrust coefficient
C_{Press}	Pressure coefficient
n	Rotating speed
P	Power
P_L	Local pressure
P_{ref}	Reference hydrostatic pressure
Q	Torque
T	Thrust
LE	Leading
TE	Trailing edge
TSR	Tip speed ratio
V	Current velocity
V_R	Resultant velocity

Greek Symbols

ρ	Density (kg/m³)
ω	Angular velocity

REFERENCES

1. Lari K., Rahmani H., Distribution tidal wave energy and its applications in coasts of Iran, J. Basic. Appl. Sci. Res., 2(1)449-460, 2012.

2. Gorji-Bandpy M., Azimi M R., Jouya M., Tidal energy and main resources in the Persian Gulf, Distributed Generation and Alternative Energy Journal, Vol. 28(2), 2013, Doi: 10.1080/21563306.2013.10677551.

3. https://www.offshore-energy.biz/simec-atlantis-redeploys-meygen-tidal-turbine (online 10 May 2024).

4. Zahedi Nejad A., Rad M., Modeling instantaneous energy exchange during rigid interaction of rotor with unsteady water flow around duct of axial tidal turbine, Modares Mechanical Engineering, Vol. 16, No. 12, pp. 692-702, 2016.

5. Gorban A N., Gorlov A M., Silantyev V M., Limits of the turbine efficiency for free fluid flow. Journal of Energy

Resources Technology, Vol. 123 (4), pp 311-317, 2001, Doi: 10.1115/1.1414137.

6. Sorensen B., Renewable energy. Second Edition, 2011, Four Volume Set, 2320 pages, https://doi.org/10.4324/9781315793245.

7. Gorlov A M, Tidal energy. Northeastern University, Boston Massachusetts, USA Academic Press Copyright, 2001.

8. Wang X., Luo X., Zhuang B., Yu W., Xu H., 6-DOF numerical simulation of the vertical-axis water turbine, ASME-JSME-KSME Joint Fluids Engineering Conference, No. AJK2011-22035, pp. 673-678, 2011, Doi: 10.1115/AJK2011-22035.

9. Whitby B., Control of an axial flow tidal stream turbine, PhD dissertation, Cardiff University, August 2013.

10. Myers L E., Bahaj A S., An experimental investigation simulating flow effects in first generation marine current energy converter arrays. Renewable Energy, Vol. 37, No. 1, pp. 28–36, 2012, Doi: 10.1016/j.renene.2011.03.043.

11. Song M., kim M C., Do I R., Rhee S., Lee J H., Hyun B S. Numerical and experimental investigation on the performance of three newly designed 100 kW-class tidal current turbines. International Journal of Naval Architecture and Ocean Engineering. 4(3): p. 241-255, 2012, https://doi.org/10.2478/IJNAOE-2013-0093.

12. Muratoglu A., Ishak Yuce M., Performance analysis of hydrokinetic turbine blade sections. Avestia Publishing Advances in Renewable Energy Volume 2, Journal ISSN: DOI: TBA, 2015.

13. Schleicher W C., Riglin J D., Kraybill Z A., Oztekin A. Design and simulation of a micro hydrokinetic turbine, Proceedings of the 1st Marine Energy Technology Symposium, METS13, Washington, USA, pp. 1-8, 2013.

14. Shojaeefard M H., Mirzaei A., Abedinejad M S., Yassi Y. Numerical study of different models of an Agnew micro hydro turbine, Modares Mechanical Engineering, Vol. 15, No. 6, pp. 221- 230, 2015.

15. Rahimian M. et al., Numerical assessment of a horizontal axis marine current turbine performance, International Journal of Marine Energy, Vol. 20, pp151-164, 2017, https://doi.org/10.1016/j.ijome.2017.07.009.

16. Shi W., Wang D., Atlar M. and Seo K C. Flow separation impacts on the hydrodynamic performance analysis of a marine current turbine using CFD. IMechE; 2013, Doi: 10.1177/0957650913499749.

17. Alipour R., Alipour R., Rahimian Koloor S S., Petrů M., Ghazanfari S A. On the performance of small-scale horizontal axis tidal current turbines. part 1: one single

turbine. Sustainability. 12, 2020. https://doi.org/10.3390/su12155985.

18. Alipour R., Alipour R., Fardian F., Rahimian Koloor S S., Moezzi R. Effect of blade pitch angle on a 2-bladed horizontal axis tidal current turbine performance, Proceedings of the 62nd International Conference of Machine Design Departments (ICMD), Atlantis Press, 2022. https://doi.org/10.2991/978-94-6463-423-5.

19. Alipour R., Alipour R., Fardian F., Tahan M H. Optimum performance of a horizontal axis tidal current turbine: A numerical parametric study and experimental validation, Energy Conversion and Management, 258, 2022, https://doi.org/10.1016/j.enconman.2022.115533.

20. de Jesus Henriques T A., Hedges T S., Owen I., Poole R J. The influence of blade pitch angle on the performance of a model horizontal axis tidal stream turbine operating under wave-current interaction, Energy, 102, 2016, http://dx.doi.org/10.1016/j.energy.2016.02.066

21. Maduka M., Li C W., Experimental evaluation of power performance and wake characteristics of twin flanged duct turbines in tandem under bi-directional tidal flows. Renew Energy; 199: 1543–1567, 2022, https://doi.org/10.1016/j.renene.2022.09.067.

22. Maduka M, Li C W., Numerical study of ducted turbines in bidirectional tidal flows. Eng Appl Comput Fluid Mech; 15: 194–209, 2021, https://doi.org/10.1080/19942060.2021.1872706.

23. Baratchi F, Jeans T L, Gerber A G, Assessment of blade element actuator disk method for simulations of ducted tidal turbines. Renew Energy; 154: 290–304, 2020.

24. Borg M G., Xiao Q., Allsop S., et al. A numerical performance analysis of a ducted, high-solidity tidal turbine. Renew Energy; 159: 663–682, 2020, https://doi.org/10.1016/j.renene.2020.04.005.

25. Lawn C J., Optimization of the power output from ducted turbines, Proceedings of the Institution of Mechanical Engineers, Part A: Journal of Power and Energy, Vol. 217, No. 1, pp. 107-117, 2003.

26. Setoguchi T., Shiomi N., Kaneko K., Development of two-way diffuser for fluid energy conversion system, Renewable Energy, Vol. 29, pp. 1757–1771, 2004, https://doi.org/10.1016/j.renene.2004.02.007.

27. Jo C H., Lee K H., Yim J Y., Rho Y H., Interaction effect analysis for tidal current power farm feasibility study applied to projects in Korea. Proceedings of the 9th European Wave and Tidal Energy Conference, Southampton, UK, 2011.

28. Shives M., Crawford C., Overall efficiency of ducted tidal current turbines. in proceedings of the Oceans 2010 MTS/IEEE Seattle Conference & Exhibition, Washington, USA, September 20–23, 2010, Doi: 10.1109/OCEANS.2010.5664426.

29. Im H., Hwang T., Kim B., Duct and blade design for small-scale floating tidal current turbine development and CFD-based analysis of power performance. J Mech Sci Tech; 34: 1591–1602, 2020, https://doi.org/10.1007/s12206-020-0321-2.

30. Tsuru W., Kinoue Y., Murakami T., et al., Design method for a bidirectional ducted tidal turbine based on conventional turbomachinery methods. Advances in Mechanical Engineering, Vol.15(6), 2023, https://doi.org/10.1177/168781322311810.

31. Ghazi M. A., Ghassemi H., Ghafari H. R., Hydrodynamic performance and the power production of the tidal turbine by new profiles at the leading-edge tubercles, Ships and Offshore Structures, 2022, https://doi.org/10.1080/17445302.2022.2078532.

32. Ghassemi H., Ghafari H. R., Homayoun E., Hydrodynamic performance of the horizontal axis tidal stream turbine using RANS solver. Zeszyty Naukowe Akademii Morskiej w Szczecinie 2018, Doi: 10.17402/298.

33. Abbasi A., Ghassemi H., Molyneux D., Numerical analysis of the hydrodynamic performance of HATST with different blade geometries. American Journal of Civil Engineering and Architecture. 6(6):236–241, 2018, doi: 10.12691/ajcea-6-6-2.

34. Abbasi A., Ghassemi H., Molyneux D., Power and thrust coefficients of the horizontal axis tidal stream turbine with different twist angles, blade numbers, and section profiles. Zeszyty Naukowe Akademii Morskiej w Szczecinie 2019, Doi: 10.17402/321.

35. Ghafari H. R., Fatahi P., Ghassemi H., Mahmoodi K., Power production of the counter-rotating tidal current turbine, including duct effect. Ships & Offshore Struct.1–13. https://doi.org/10.1080/17445302.2021.2021605.